Accepted Manuscript

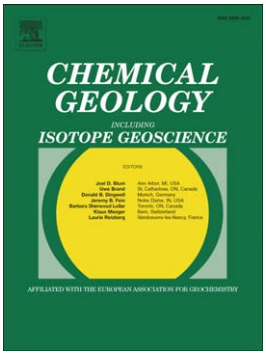

U-Pb SHRIMP geochronology of zircon from the Catoca kimberlite, Angola: Implications for diamond exploration

Sandra E. Robles-Cruz, Monica Escayola, Simon E. Jackson, Salvador Galí, Vladimir Pervov, Manuel Watangua, Antonio Gonçalves, Joan Carles Melgarejo

PII: S0009-2541(12)00167-2
DOI: doi: 10.1016/j.chemgeo.2012.04.001
Reference: CHEMGE 16498

To appear in: *Chemical Geology*

Received date: 9 August 2011
Revised date: 2 April 2012
Accepted date: 4 April 2012

Please cite this article as: Robles-Cruz, Sandra E., Escayola, Monica, Jackson, Simon E., Galí, Salvador, Pervov, Vladimir, Watangua, Manuel, Gonçalves, Antonio, Melgarejo, Joan Carles, U-Pb SHRIMP geochronology of zircon from the Catoca kimberlite, Angola: Implications for diamond exploration, *Chemical Geology* (2012), doi: 10.1016/j.chemgeo.2012.04.001

This is a PDF file of an unedited manuscript that has been accepted for publication. As a service to our customers we are providing this early version of the manuscript. The manuscript will undergo copyediting, typesetting, and review of the resulting proof before it is published in its final form. Please note that during the production process errors may be discovered which could affect the content, and all legal disclaimers that apply to the journal pertain.

ACCEPTED MANUSCRIPT

U-Pb SHRIMP geochronology of zircon from the Catoca kimberlite, Angola: Implications for diamond exploration

Sandra E. Robles-Cruz[a,*], Monica Escayola[b], Simon E. Jackson[c], Salvador Galí[a], Vladimir Pervov[d], Manuel Watangua[e], Antonio Gonçalves[e], Joan Carles Melgarejo[a]

[a]*Department de Cristal•lografia, Mineralogia i Dipòsits Minerals, Universitat de Barcelona, Martí i Franquès s/n, 08028 Barcelona, Spain (sandra_robles@ub.edu)*

[b]*CONICET-IDEAN Instituto de Estudios Andinos, Laboratorio de Tectónica Andina, Universidad de Buenos Aires, C1033AAJ Capital Federal, Argentina*

[c]*Geological Survey of Canada, 601 Booth Street, Ottawa, K1A 0E8 Ontario, Canada*

[d]*Sociedade Mineira de Catoca, Catoca, Lunda Sul, Angola*

[e]*Departamento de Geologia, Universidade Agostinho Neto, Av. 4 de Fevereiro 7, 815 Luanda, Angola*

ACCEPTED MANUSCRIPT

Abstract

We present the first age determinations of zircon from the diamondiferous Catoca kimberlite in northeastern Angola, the fourth largest kimberlite body in the world. The U-Pb ages were obtained using a Sensitive High Resolution Ion Microprobe II (SHRIMP II) on zircon crystals

ACCEPTED MANUSCRIPT

derived from tuffisitic kimberlite rocks and heavy-mineral concentrates from the Catoca kimberlite. The SHRIMP results define a single weighted mean age of 117.9 ± 0.7 Ma (Mean square weighted deviation MSWD = 1.3). More than 90% of the results indicate a single age population. There is no evidence for variable ages within single crystals, and no diffusional profiles are preserved. These data are interpreted as the maximum age of the kimberlite eruption at Catoca. The U/Th values suggest at least two different sources of zircon crystals. These different populations may reflect different sources of kimberlitic magma, with some of the grains produced in U- and Th- enriched metasomatized mantle units. This idea is consistent with the two populations of zircon identified in this study. One population originated from a depleted mantle source with low total REE (less than 25 ppm), and the other was derived from an enriched source, likely from the mantle or a carbonatite-like melt with high total REE (up to 123 ppm).

The tectonic setting of northeastern Angola is influenced by the opening of the south Atlantic, which reactivated deep NE-SW-trending faults during the early Cretaceous. The eruption of the Catoca kimberlite can be correlated with these regional tectonic events. The Calonda Formation (Albian-Cenomanian age) is the earliest sedimentary unit that incorporates eroded material derived from the diamondiferous kimberlites. Thus, the age of the Catoca kimberlite eruption is restricted to the time between the middle of the Aptian and the Albian. The new interpretation will be an important guide in future exploration for diamonds because it provides precise data on the age of a diamond-bearing kimberlite pulse in Angola.

Components: 5,381 words, 7 figures, 4 tables.

ACCEPTED MANUSCRIPT

Keywords: U-Pb dating; SHRIMP; Geochronology; Zircon; Diamond; Catoca kimberlite

* Corresponding author. Tel.: +506 8839 3981; fax: +506 2242 4411

E-mail addresses: sandra_robles@ub.edu; sandrarobc@gmail.com (S.E. Robles-Cruz)

ACCEPTED MANUSCRIPT

ACCEPTED MANUSCRIPT

1. Introduction

Kimberlites contain primary minerals crystallized from a kimberlitic magma, a suite of mega- and macrocrysts (e.g., zircon, diamond), and a complex variety of xenoliths (e.g., peridotite). According to previous studies (Moore et al., 1992; Griffin et al., 2000; Pivin et al., 2009; and references therein), some zircon megacrysts (crystals larger than 1 cm) do crystallize from fractionating magmas in the mantle, are intergrown with other megacryst phases (ilmenite, phlogopite, high-Fe olivine), and contain inclusions of chromian diopside, chromite, and diamond. Mantle-derived zircon megacrysts have trace element compositions that are distinct from zircon derived from the crust. These megacrysts have lower U and Th concentrations, and a lower total abundance of rare-earth elements (REE) than zircon of crustal derivation (Belousova et al., 2002; Heaman et al., 2006; and references therein). The U-Pb dating of zircon is by far the most widely used method for obtaining reliable mineral-growth ages from different types of rocks. Zircon can provide reliable ages because of its resistance to thermal disturbances. However, the dating of kimberlites is one of the most difficult applications of this method because crystal growth may have occurred hundreds of millions of years before kimberlite emplacement.

The aim of this study is to determine the U-Pb ages of zircon from the diamondiferous Catoca kimberlite, in the Lunda Sul province of Angola, using a Sensitive High Resolution Ion Microprobe II (SHRIMP II). The study contributes to a better understanding of the geological evolution of the Catoca kimberlite, which has important implications for diamond exploration. Trace-element analyses carried out by Laser Ablation - Inductively Coupled Plasma - Mass Spectrometry (LA-ICP-MS) were used to determine the chemical composition of the zircon (including the REE) from the kimberlite and to suggest potential sources of the zircon. We also

ACCEPTED MANUSCRIPT

present a comparison of the Catoca kimberlite with kimberlites in southeastern Brazil that were formed during the Early Cretaceous.

1.1 Background information and previous geochronological research in Angola

The kimberlites of Angola are distributed in clusters (Pereira et al., 2003; Egorov et al., 2007) in the northeastern, central, and southwestern areas of the country. Most of the kimberlites are concentrated within the Lucapa structure, with a NE-SW orientation, or along NW-SE faults (Fig. 1). The Lucapa structure is a major basement fault system with the highest diamondiferous potential in Angola (Pereira et al., 2003). The Catoca kimberlite, the fourth largest kimberlite pipe in the world (639,000 m^2), is located in the northeastern part of this structure, and exhibits rocks of crater and diatreme facies.

In the earliest geochronological studies, Bardet and Vachette (1966) proposed a main Cretaceous kimberlitic event in the Congo craton based on stratigraphic relationships. Subsequently, Davis (1977) dated one crystal of zircon from the Val do Queve kimberlite, located in the central part of Angola by conventional U-Pb TIMS analysis. He reported a ^{206}Pb-^{238}U age of 134.0 ± 2.0 Ma. However, Davis noted some unspecified analytical problems, which he attributed to the crystal's low U content. Later, Haggerty et al. (1983) carried out fission-track dating of zircon from the same area and reported an age of 133.4 ± 11.5 Ma, which they interpreted as the time of eruption of the Val do Queve kimberlite. In contrast, Egorov et al. (2007) published a K-Ar date of 372 ± 8 Ma for phlogopite from the groundmass of the Chicuatite kimberlite in southwestern Angola and interpreted it as the kimberlite age. Eley et al. (2008) reported a ^{206}Pb/^{238}U age for zircon from the Alto Cuilo 55 kimberlite and the Alto Cuilo

ACCEPTED MANUSCRIPT

197 kimberlite (each date was based on a single-point analysis) of 113.0 ± 0.8 Ma. The same authors reported $^{206}Pb/^{238}U$ ages for perovskite from the Alto Cuilo 139 kimberlite of 135.7 ± 2.1 Ma and from the Alto Cuilo 1 kimberlite of 145.1 ± 4.0 Ma (the authors did not specify the technique that was used), and a Rb-Sr age for phlogopite from the Alto Cuilo 254 kimberlite of 115.5 ± 1.1 Ma. All of the Alto Cuilo kimberlites are a part of the Luxinga kimberlite cluster, located ca. 85 km southwest of Catoca. According to Eley et al. (2008), the ages indicate that kimberlite intrusive activity took place in the Luxinga cluster between approximately 145 and 113 Ma. Recently, Jelsma et al. (2012) reported U-Pb ages for zircon from kimberlites in central Angola between 252 and 216 Ma (median age of 235 Ma), using LA-ICP-MS. The authors interpreted these data as a new age population of kimberlite emplacement in Angola.

2. Geological setting

The geological history of Angola includes the following three major phases, which have shaped the country (De Carvalho et al., 2000; Guiraud et al., 2005; Egorov et al., 2007): (1) the Archean orogeny; (2) the Proterozoic orogenic cycles (Eburnian: Paleoproterozoic, Kibaran: Mesoproterozoic, and Pan-African: Neoproterozoic); and (3) the deposition of Phanerozoic sedimentary sequences resting unconformably on previously eroded surfaces (Pereira et al., 2003). The subsequent break-up of Gondwana during the Jurassic to Cretaceous, between 190 and 60 Ma (e.g., Jelsma et al., 2004), caused the development of basins that are associated with deep fault systems in Angola. These fault systems facilitated the emplacement of alkaline, carbonatitic, and kimberlitic magmas (Pereira et al., 2003).

ACCEPTED MANUSCRIPT

The Late Cretaceous regional extension was associated with older deep-seated faults and "grabens" with NE-SW and NW-SE trends (Jelsma et al., 2009). An example of such a NE-SW trend is the Lucapa deep-seated fault system, which developed a local basin in northeastern Angola along a line that continues southwest to a transform fault of the Mid-Atlantic Ridge (White et al., 1995). The Lucapa structure has been a belt of recurring tectonic weakness since the Paleoproterozoic (Jelsma et al., 2009). Most of the diamondiferous kimberlites in Angola are located along the Lucapa structure in northeastern Angola, although it is not clear whether kimberlites were emplaced at the time of rifting or whether they resulted from post-rifting events. Strike-slip and shear fault systems in northeastern Angola likely could have led to decompression (local extension) and compression, resulting in some control on the distribution of igneous activity within the Lucapa structure. These processes could also have different expressions within the Angolan Shield and Kasai Craton. Reliable age determinations are very important for understanding the timing of these intracontinental processes. In the southwestern part of Angola, there are outcrops of undersaturated alkaline rocks and carbonatites along this trend (Reis, 1972), as well as some minor kimberlite fields (Egorov et al., 2007).

Continental sediments that unconformably overlie the Precambrian basement filled the Lucapa structure during the Cretaceous and Paleogene. An example of this package of sediments is the Calonda Formation, a fining upward lithostratigraphic unit of the Kwango Group that was formed by torrential deposits gradually changing to lagoonal facies and concluding with low-energy deposits associated with aeolian episodes. The Calonda Formation is the oldest sedimentary unit in Angola that contains detrital diamond and kimberlite clasts (Pereira et al., 2003; and references therein). It is reported to be Albian to Cenomanian in age, based on fish

ACCEPTED MANUSCRIPT

macrofossils, palynomorphs, and tectonostratigraphic studies (Pereira et al., 2003). It has become an important target in the exploration for alluvial diamond deposits.

3. Sample description

In this study, nineteen crystals of zircon between 0.6 and 4 mm in length were taken from three core samples (four crystals) of tuffisitic kimberlites (TK) and three samples (fifteen crystals) of heavy-mineral concentrate from the Catoca kimberlite to perform the SHRIMP analyses (Table 1). The TK have macrocrysts (0.5-10 mm) of olivine (35-50 modal %), which are, in most cases, completely replaced by serpentine, calcite, and saponite. Xenoliths of the host rocks (3-5 modal %), comprising gneiss and amphibolites, are common. Also present are mantle xenoliths (1-5 modal %) (e.g., altered metasomatized peridotite) and xenoliths of carbonatite (calcite + anhedral Mn-rich ilmenite + zircon + apatite + phlogopite). Garnet (G9 and G10, Grüttter et al., 2004), chromian diopside, ilmenite, amphibole, phlogopite, and zircon are found as mega- and macrocrysts in an altered kimberlite groundmass. Some zircon crystals exhibit a reaction rim of baddeleyite. The matrix of the TK rocks contains lizardite, apatite, calcite, ilmenite, and chromite. Titanite, zirconolite, baddeleyite, barite, dolomite, witherite, barytocalcite, strontianite, and sulfides have also been identified in the matrix by quantitative powder X-ray diffraction (powder method) and quantitative chemical analyses using an electron-microprobe (EMP) (Robles-Cruz et al., 2009). One additional zircon crystal derived from a heavy-mineral concentrate from the Tchiuzo kimberlite (15 km north of the Catoca kimberlite) was added to this study for comparative purposes.

ACCEPTED MANUSCRIPT

Large grain-size is a characteristic feature of zircon from kimberlites. According to several authors (e.g., Belousova et al., 1998), zircon crystals found in kimberlites are relatively large in size (several millimeters) compared to most zircon crystals from other types of igneous rock or from metamorphic rocks. These crystals vary in color from colorless to brownish yellow. The twenty crystals analyzed in this study are characterized by an almost complete absence of crystal faces, and most of them are angular to subangular, presumably as a result of fracturing. A few of them are subrounded, likely owing to disequilibrium with the medium, causing incipient resorption during interaction with the kimberlitic magma.

According to back-scattered electron (BSE) images, the twenty zircon crystals are homogeneous at the major element level. The crystals do not exhibit evidence of metamictization. Nineteen of the twenty crystals exhibit oscillatory zoning in cathodoluminescence (CL) (Figs. 2B, C, D, and F), which is usually interpreted to be a result of crystallization in a melt or fluid (Belousova et al., 1998; Liati et al., 2004; Page et al., 2007). Crystal no. 18 has dark-CL growth zoning (Fig. 2E), which is indicative of high U content. Four zircon crystals in the analyzed set exhibit partial replacement by baddeleyite (ZrO_2) along the borders. In addition, these crystals are fractured, and the resulting fracture surfaces are not corroded by baddeleyite (Figs. 2A, B). The baddeleyite crystals are irregular and narrow between 10 and 40 μm in breadth.

Three representative crystals (nos. 19, 21, and 22), between 1 and 3 mm in length and picked from the heavy-mineral concentrate of the Catoca TK, were analyzed with an LA-ICP-MS. These zircon crystals exhibit oscillatory zoning in CL. One of these crystals was also analyzed with SHRIMP (no. 19).

ACCEPTED MANUSCRIPT

4. Analytical methods

4.1 Determinations of trace element concentrations

Trace-element analyses were carried out by LA-ICP-MS on three zircon crystals (nos. 19, 21, and 22) from the Catoca kimberlite at the Geological Survey of Canada. The trace-element determinations were performed using a New Wave Research UP213 laser-ablation system in combination with a Perkin Elmer 6100DRC quadrupole inductively coupled plasma mass spectrometer. The data acquisition and calibration protocols employed have been described by Longerich et al. (1996) and Jackson (2008). Operating conditions and data-acquisition parameters used in this study are summarized in Table 2. Data reduction was performed using the software GLITTER 4.4.2 (Griffin et al., 2008). The standard NIST SRM 610 (synthetic glass reference material, National Institute of Standards and Technology) was used as the primary calibration standard using concentration values from GEOREM (http://georem.mpch-mainz.gwdg.de/, data downloaded February 24, 2010). The stoichiometric SiO_2 content of 32.8% was used for internal standardization to correct differences in ablation yield between the sample and reference material. A secondary standard, BCR-2G (a homogeneous basaltic reference glass prepared by the U.S. Geological Survey: Jochum and Stoll, 2008), was used to monitor the precision and accuracy of the technique. Precision and accuracy were assessed from repeated analyses of the BCR-2G standard and were usually better than 10% for concentrations at the ppm level. Detection limits were better than ~0.06 ppm for all elements reported, with the exception of Ti.

ACCEPTED MANUSCRIPT

4.2 U-Pb dating

The zircon crystals were mounted in epoxy along with fragments of laboratory standard zircon z6266 ($^{206}Pb/^{238}U$ age = 559 Ma) at the Geological Survey of Canada. The mid-sections of the zircon crystals were exposed and characterized in back-scattered electron (BSE) mode utilizing a Zeiss Evo 50 scanning electron microscope and a cold cathodoluminescence stage mounted on a petrographic microscope to study internal features within the crystals, such as zoning and structures. The surfaces of the 2.5-cm mounts were evaporatively coated with 10 nm of high-purity Au.

The U-Pb analyses were conducted at the Geochronology Laboratory, Geological Survey of Canada (Ottawa), using a Sensitive High Resolution Ion Microprobe II (SHRIMP II). Analyses were performed using an $^{16}O^-$ primary beam, projected onto the zircon crystals at 10 kV with a beam current of ca. 10 nA. The sputtered area used for analysis was ca. 25 µm in diameter. The count rates at ten masses including background were sequentially measured over six scans with a single electron multiplier with a deadtime of 27 ns. Off-line data processing was accomplished using the SQUID 2.22.08.04.30 software, rev. 30 Apr 2008. The 1σ external errors of the $^{206}Pb/^{238}U$ ratios reported in the table of data (Table 4) incorporate a ±1.1% error in calibrating the standard zircon (see Stern and Amelin, 2003). For the common Pb correction, we utilized the Pb composition of the surface blank. No fractionation correction was applied to the Pb-isotope data. The ^{207}Pb method (Williams, 1998) was used to calculate $^{206}Pb/^{238}U$ ages and errors.

5. Results

5.1 REE and Ti-in zircon thermometry

ACCEPTED MANUSCRIPT

On the basis of total REE concentrations in zircon from the Catoca kimberlite, we identified two ranges of values. One set consisted of total REE concentrations of less than 25 ppm, and the other set was characterized by total REE concentrations up to 123 ppm (Table 3). The zircon from the Catoca kimberlite (Fig. 3) exhibits low concentrations of light REE (LREE), a positive anomaly in Ce (chondrite-normalized value up to 10.04 ppm, 9.6 ppm absolute concentration), a lack of an Eu anomaly, and a positive slope from Pr to Lu, which flattens toward the heavy REE (HREE). Similar chondrite-normalized patterns and REE contents have been observed in zircon crystals from other kimberlites in southern Africa, Yakutia, and Australia (Belousova et al., 1998, 2001).

The REE patterns in zircon indicate that HREE and Ce^{4+}, with a much more compatible ionic radius (0.97 Å) compared to Ce^{3+} (1.18 Å), are preferentially incorporated in the zircon structure (Ballard et al., 2002; Hoskin and Schaltegger, 2003). This anomalous abundance of Ce^{4+} could be the result of an increased Ce^{4+}/Ce^{3+} value in the melt as a function of high oxygen fugacity (Belousova et al., 2002; Hoskin and Schaltegger, 2003; Whitehouse and Platt, 2003; and references therein). Similarly, the absence of an Eu anomaly may be caused by a high Eu^{3+}/Eu^{2+} value under oxidized magma conditions in a feldspar-free magmatic environment (Hoskin and Schaltegger, 2003). The suggestion of relatively high oxygen fugacity (fO_2) conditions during zircon crystallization seems more favorable for an interpretation of a positive Ce anomaly combined with the absence of a negative Eu anomaly.

Concentrations of yttrium exhibit distinct ranges of values for each zircon population (Table 3). In one population, Y concentrations are between 39 and 120 ppm, while higher Y concentrations, between 330 and 480 ppm, are found in the other population. Concentrations of

ACCEPTED MANUSCRIPT

Hf are between 9580 and 13700 ppm for the first population and between 9180 and 9970 ppm for the second population of zircon.

These three zircon crystals exhibit low Ti concentration, between 3.4 and 10.9 ppm, for the first population and between 1.17 and 2.66 ppm for the second population. There is no direct evidence that these zircon crystals coexisted with a Ti-dominant phase. However, ilmenite is usually found in xenoliths, as mega- and macrocrystals, and in the groundmass of the Catoca kimberlite.

The Ti-in-zircon thermometer (Watson et al., 2006) was applied to calculate the temperature at which the zircon crystallized. The calculated temperatures are between 600 and 750 ºC, which is very low for a kimberlite. One possible explanation for this result is the lack of coexistence of zircon with a Ti-dominant phase, which leads to uncertainty in the activity coefficient of Ti. The same problem has been reported previously, where some doubts have been raised about the applicability of the Ti-in-zircon thermometer for zircon from kimberlites (Page et al., 2007).

ACCEPTED MANUSCRIPT

5.2 SHRIMP U-Pb ages

Forty-one SHRIMP analyses were performed on 19 zircon crystals from the Catoca kimberlite. Table 4 summarizes the results of all the SHRIMP analyses. Concentrations of Th and U range between 1 and 654 ppm and between 6 and 326 ppm, respectively. These ranges of values, along with the REE analyses, appear to support the idea that the zircon crystals originated from different sources. The Th/U values range from 0.21 to 2.07. Several analyses show very low U concentrations and very high proportions of common Pb, up to 45%. The large amount of common Pb is evident in a Tera-Wasserburg plot (Fig. 5). Samples with common Pb

ACCEPTED MANUSCRIPT

concentrations of greater than 15% have higher $^{206}Pb/^{238}U$ ages, which is attributed to uncertainties that result from the very large common Pb correction required in those cases. For this reason, all results with common Pb proportions greater than 15% were excluded from interpretations (7 of 41 analyses rejected, Fig. 4). The 34 analyses below the 15% cut-off value define a single weighted mean age of 117.9 ± 0.7 Ma (Mean square weighted deviation MSWD = 1.3, probability 0.093, Fig. 4B). Quadratic addition of the systematic error in the mount calibration (0.3% 1 sigma) gives a total error estimate of 117.9 ± 0.7 Ma.

Five SHRIMP analyses were carried out on one zircon crystal (no. 20) from the Tchiuzo kimberlite, for comparison with the results discussed above. Concentrations of Th range between 11 and 34 ppm, and concentrations of U range from 36 to 61 ppm. The Th/U values range between 0.30 and 0.56. The weighted mean of the five analyses gives an age of 121 ± 3 Ma (MSWD = 1.6; probability of fit 0.17). Two analyses have common Pb contents above 15%; if these are rejected, the remaining three analyses have an identical weighted mean age of 121.2 ± 1.8 (MSWD = 0.86; probability of fit 0.45). Thus, the single crystal from the Tchiuzo kimberlite yields an age slightly older than the weighted mean age obtained for the Catoca kimberlite.

6. Discussion

6.1 Different sources of zircon

The zircon crystals have well-defined characteristic features in their chondrite-normalized patterns, total REE abundances (Fig. 3), and different U and Th concentrations (Table 3). On the basis of their REE composition, two different populations of zircon crystals have been identified in the Catoca kimberlite. The first population is characterized by a low concentration of REE

ACCEPTED MANUSCRIPT

(less than 25 ppm), U (less than 30 ppm), Th (less than 10 ppm), and Th^{zrn}/U^{zrn} values (0.20-0.37). Experimental and theoretical studies in mafic and ultramafic rocks indicated that in such rocks, U^{zrn}/U^{melt} is approximately 100 and $(Th/U)^{zrn\text{-}melt}$ equals approximately 0.17 (Blundy and Wood, 2003). On the basis of results obtained in this study ($Th^{zrn}/U^{zrn} \approx 0.26$, Table 4), we estimate a Th^{rock}/U^{rock} value between 2.1 and 3.6 for the 'first' population of zircon. This value is within the limits proposed by Zartman and Richardson (2005), between ~4 and ~2, for depleted asthenosphere over the last 2.5 Ga. This first population of zircon crystals could be genetically linked to the kimberlite. The second population is characterized by high concentrations of REE (up to 123 ppm), high Th (more than 45 ppm), and high U (more than 100 ppm). This population is likely derived from an enriched source.

These two populations of primary zircon were produced by at least two different batches of magma that exhibit very similar ages (Fig. 6). The first population is similar in Th/U values to the zircon megacrysts typically found in kimberlites (Heaman et al., 2006), and the second is close to those reported from xenoliths of glimmerite (Rudnick et al., 1998) or MARID (Kinny and Dawson, 1992; Hamilton et al., 1998). Both populations of zircon crystals are corroded and overgrown by a rim of baddeleyite. The presence of such a rim suggests a desilication reaction as a result of the interaction of zircon with carbonate in the kimberlitic magma, for example:

$$ZrSiO_4 + (Ca, Mg)CO_3 \rightarrow ZrO_2 + (Ca, Mg)\text{silicate} + CO_2$$

or as a result of a reaction with other minerals in a carbonated kimberlitic melt, as has been noted in other kimberlites (Haggerty, 1991; Dawson et al., 2001; Page et al., 2007). In addition, the crystals were fragmented after the development of the baddeleyite rim because the broken surfaces are never replaced by baddeleyite (Figs. 2A, 2B). Therefore, these crystals may have

ACCEPTED MANUSCRIPT

been replaced along the borders and then fractured during eruption or later, such as during treatment in the gridding mill.

6.2 Age data

Two interpretations are possible to explain the presence of the SHRIMP U-Pb zircon ages obtained in this study. The first interpretation is that they reflect a period of zircon growth at 117.9 ± 0.7 Ma, which would represent a maximum eruption age for the Catoca kimberlite. The second interpretation is that the zircon crystals partially retain an older, inherited component that was incompletely reset by diffusive Pb-loss prior to eruption at 117.9 ± 0.7 Ma. Did the zircon form prior to kimberlite eruption but fail to quantitatively retain Pb owing to high ambient temperatures and diffusive loss of Pb?

The Pb closure temperature of zircon is in excess of 900 ºC (Cherniak and Watson, 2000; Heaman et al., 2006; and references therein). Thus, the zircon thus likely records the time when it was transported from the mantle by the kimberlitic magma. Although exposure to mantle temperatures for long periods of time will cause zircon to lose Pb through diffusion, several investigators of zircon in kimberlitic rocks (Mezger and Krogstad, 1997; Belousova et al., 2001; Cherniak and Watson, 2003) have suggested that a complete resetting does not invariably take place. Specifically, according to Belousova et al. (2001), zircon crystals may retain radiogenic Pb at lithospheric mantle temperatures between 600 and 1200 ºC.

The estimated geotherm for the Catoca kimberlite (Robles-Cruz et al., in preparation), calculated from data on garnet peridotite xenoliths generated using the Nimis and Taylor (2000) geothermobarometer, gives a temperature between 900 and 1200 ºC at 40-55 kbar (160-200 km,

ACCEPTED MANUSCRIPT

in the subcratonic lithospheric mantle). At this range of temperatures, the calculated volume diffusion of Pb in zircon using the Arrhenius relation (Cherniak and Watson, 2000) is between 3.23×10^{-26} at 900 ºC and 3.14×10^{-21} m^2/s^{-1} at 1200 ºC. Calculations of Pb diffusion in zircon (D_{Pb}) give:

$$D_{Pb} = 1 \times 10^{-1} \exp(-550 \text{ kJ mol}^{-1}/RT) \text{ m}^2 \text{ s}^{-1} \text{ , } R = 8.314472 \times 10^{-3} \text{ (gas constant)}$$

$$D_{Pb} = 3.23 \times 10^{-26} \text{ m}^2/\text{s}^{-1}, \text{ at } T = 1173 \text{ K (900 ºC)}$$

$$D_{Pb} = 3.14 \times 10^{-21} \text{ m}^2/\text{s}^{-1}, \text{ at } T = 1473 \text{ K (1200 ºC)}$$

This Pb diffusion is not significant and precludes the second interpretation.

Other studies (Schärer et al., 1997; Corfu et al., 2003) suggest that zircon keeps a record (partial or complete) of one or more thermal events that it has experienced. Thus each zircon crystal is telling an "individual" history and the measured U-Pb zircon ages, together with the REE concentrations, provide insight into different episodes of crystallization.

6.3 Geotectonic implications

This new interpretation of a maximum age for the kimberlitic eruption at 118 ± 1 Ma (Aptian age) is consistent with the regional tectonostratigraphy of northeastern Angola (Fig. 7). The Catoca kimberlite was expected to be younger than the carbonatites and alkaline rocks found in the Lucapa structure. These rocks yielded K-Ar and Rb-Sr ages between 138 and 130 Ma (Alberti et al., 1999; and references therein). The U-Pb ages obtained in this study are similar to those reported for the Alto Cuilo kimberlites (Eley et al., 2008; and references therein), which

ACCEPTED MANUSCRIPT

are slightly older than the Calonda Formation and contain eroded fragments of diamondiferous kimberlite.

Cretaceous kimberlitic events of similar age have also been reported in the São Francisco craton (Brazil), the Kaapvaal craton (South Africa and Botswana), and the Congo-Kasai craton (the Democratic Republic of Congo), which were all part of Gondwanaland (e.g., Batumike et al., 2007; Jelsma et al., 2009). Systems of deep faults present in these cratons probably were the focus of thermal perturbations and injection of melt. The Canastra 01 kimberlite in Brazil, located at the border of the São Francisco craton (Da Costa, 2008), yielded an age of 120 ± 10 Ma using K/Ar in phologopite (Chaves et al., 2008; and references therein). It is associated with a NE-SW general tectonic trend and considered to be related to lithospheric heating that took place before rifting (Fleischer, 1998; Read et al., 2004), at a time when the presence of the Tristan da Cunha mantle plume (133 Ma) would have exerted tectonic control (Wilson, 1992). In the western part of the Kaapvaal craton, in South Africa, kimberlites with ages of ca. 120 Ma (Jelsma et al., 2009; and references therein) are associated with NE-SW preferential tectonic orientation. In the Congo-Kasai craton, the reported ages of the earliest episodes of kimberlitic magmatism are between 116 and 70 Ma (Batumike et al., 2009; and references therein), where NE-SW and E-W general tectonic trends have been identified. The youngest kimberlitic magmatic episode reported, the Mbuji-Mayi kimberlites (70 Ma, Schärer et al., 1997), located in the east Kasai province in the Democratic Republic of Congo, have an E-W trend. The implication is that there was a change in the tectonic direction with which these kimberlites are associated between 120 and 70 Ma, around the end of the Early Cretaceous.

Our interpretation of 118 ± 1 Ma for the maximum age of the kimberlitic eruption in Catoca, which is associated with a NE-SW tectonic trend (Lucapa structure), reinforces the hypothesis of

ACCEPTED MANUSCRIPT

Jelsma et al. (2009) that 120 Ma (Aptian age) kimberlites are preferentially associated with NE-SW tectonic trends, whereas 85 Ma (Santonian age) kimberlites are emplaced in E-W lineaments. Our finding of an Aptian age for the maximum age of the kimberlitic eruption in Catoca is also consistent with a single model for the magmatic province, which extends over what is now southeastern Brazil and southwestern Africa, coincident with the opening of the South Atlantic Ocean (Hawkesworth et al., 1992, 1999; Guiraud et al., 2010). The extensional tectonic setting, rifting, and opening of the South Atlantic during the Early Cretaceous (Pereira et al., 2003; Jelsma et al., 2009) and the reactivation of deep-seated fault systems probably contributed to lithospheric heating (mantle upwelling) and, ultimately, to kimberlitic magmatism in Angola.

7. Conclusions

(1) On the basis of U-Pb-derived zircon dates, petrographic and cathodoluminescence imaging studies, REE data, and the regional geological setting, we conclude that the maximum age for the Catoca kimberlite eruption is 118 ± 1 Ma, which is an Aptian age. Almost all of the analyses in this study belong to a single age population, with no evidence for variable ages within single crystals and no diffusional profiles preserved.

(2) The U/Th values suggest at least two different sources of zircon crystals. Some of the zircon crystals could have been produced in U-Th-enriched metasomatized mantle units (MARID or glimmeritic suite assemblages), while others have chemistries suggestive of a depleted asthenosphere source. Hence, these different populations can reflect different sources for the kimberlitic magma.

ACCEPTED MANUSCRIPT

(3) The presence of different sources of zircon is consistent with the two populations of zircon also identified based on REE abundances. These populations are characterized either by zircon crystals originating from a depleted mantle source with low concentration of REE (less than 25 ppm) or by zircon crystals derived from an enriched source, likely a carbonatitic melt, with high concentrations of REE up to 123 ppm.

(4) The age of the Catoca kimberlite is restricted to between 118 ± 1 Ma (the maximum age for the kimberlite eruption in Catoca) and 112 Ma, the beginning of deposition of diamondiferous clasts in the Calonda Formation. The eruptive event for the Catoca kimberlite appears to have taken place in this range of ages.

(5) The diamondiferous Catoca kimberlite seems to be tectonically related to other Early Cretaceous kimberlites confined in NE-SW lineaments in southwestern and southern Africa. This is consistent with an incipient rifting stage previously proposed by Jelsma et al. (2009) between 135 and 115 Ma. This understanding has important implications for diamond exploration. The documentation concerning the maximum age of eruption of the Catoca kimberlite during the Aptian provides precise data on the age of a diamond-bearing kimberlite pulse in Angola and should act as an important guide for diamond exploration.

ACCEPTED MANUSCRIPT

Acknowledgments

We acknowledge the great contribution of Dr. Bill Davis to the analytical work. We thank Dr. Anthi Liati and two more anonymous reviewers, as well as the editor, Dr. Klaus Mezger, for their excellent revision of this manuscript and their valuable comments. We greatly appreciate the revision and improvements of Prof. Robert F. Martin to this manuscript. This research is

ACCEPTED MANUSCRIPT

funded by the CGL2006-12973 and CGL2009-13758 BTE projects of Ministerio de Educación y Ciencia (Spain), and the AGAUR SGR 589 and SGR444 of the Generalitat de Catalunya. The first author (SERC) received an FI grant and a BE grant, both sponsored by the Departament d'Educació i Universitats de la Generalitat de Catalunya and the European Social Fund. We thank ENDIAMA, which kindly allowed SERC to acquire samples for her PhD thesis and allowed the use of all facilities for the mine trip. We acknowledge the Geological Survey of Canada (GSC), Ottawa, for all of the support during a six-month Volunteer Assistant visit of SERC, and we thank the Laboratories of Geochemistry and Geochronology (GSC), especially Tom Pestaj, for his collaboration and assistance during the preparation and analysis of samples. The authors also thank the Serveis Cientificotècnics de la Universitat de Barcelona for assistance in the use of SEM/ESEM-BSE-EDS analyses (E. Prats. and J. García Veigas).

References

Alberti, A., Castorina, F., Censi, P., Comin-Chiaramonti, P., Gomes, C.B., 1999. Geochemical characteristics of Cretaceous carbonatites from Angola. J. Afr. Earth Sci. 29 (4), 735-759.

Ballard, J.R., Palin, J.M., Campbell, I.H., 2002. Relative oxidation states of magmas inferred from Ce(IV)/Ce(III) in zircon: application to porphyry copper deposits of northern Chile. Contrib. Mineral. Petrol. 144, 347-364.

Bardet, M.G., Vachette, M., 1966. Détermination d'âges de kimberlites de l'Ouest Africain et essai d'interprétation des datations des diverses venues diamantifères dans le monde. Bureau de Recherches Géologiques et Minières, Département Minéralogie, Pétrographie, Métallogènie, Géochimie. Rep. No. DS. 66 A 69, Paris, pp. 20.

ACCEPTED MANUSCRIPT

Batumike, J.M., O'Reilly, S.Y., Griffin, W.L., Belousova, E.A., 2007. U–Pb and Hf-isotope analyses of zircon from the Kundelungu Kimberlites, D.R. Congo: Implications for crustal evolution. Precambrian Res.156 (3-4), 195-225.

Batumike, J.M., Griffin, W.L., O'Reilly, S.Y., Belousova, E.A., Pawlitschek, M., 2009. Crustal evolution in the central Congo-Kasai Craton, Luebo, D.R. Congo: Insights from zircon U-Pb ages, Hf-isotope and trace-element data. Precambrian Res. 170 (1-2), 107-115.

Belousova, E.A., Griffin, W.L., O'Reilly, S.Y., Fisher, N.I., 2002. Igneous zircon: Trace element composition as an indicator of source rock type. Contrib. Mineral. Petrol. 143 (5), 602-622.

Belousova, E.A., Griffin, W.L., Pearson, N.J., 1998. Trace element composition and cathodoluminescence properties of southern African kimberlitic zircons. Mineral. Mag. 62A (3), 355-366.

Belousova, E.A., Griffin, W.L., Shee, S.R., Jackson, S.E., O'Reilly, S.Y., 2001. Two age populations of zircons from the Timber Creek kimberlites, Northern Territory, as determined by Laser-ablation ICP-MS analysis. Aust. J. Earth Sci. 48 (5), 757-766.

Blundy, J., Wood, B., 2003. Mineral-melt partitioning of Uranium, Thorium and their daughters, in: Bourdon, B., Ribe, N.M., Stracke, A., Saal, A.E., Turner, S.P. (Eds.), Uranium-Series Geochemistry. Rev. Mineral. Geochem., vol. 52, 59-123.

Chaves, M.L.S.C., Benitez, L., Brandão, P.R.G., Girodo, A.C., 2008. Kimberlito Canastra-1 (São Roque de Minas, MG): geologia, mineralogia e reservas diamantíferas. REM, Rev. Esc. Minas 61 **(**3), 57-364.

Cherniak, D.J., Watson, E.B., 2000. Pb diffusion in zircon. Chem. Geol. 172, 5-24.

ACCEPTED MANUSCRIPT

Cherniak, D.J., Watson, E.B., 2003. Diffusion in zircon, in: Hanchar, J.M., Hoskin, P.W.O. (Eds.), Zircon. Rev. Mineral. Geochem., v. 53, pp. 113–143.

Corfu, F., Hanchar, J.M., Hoskin, P.W.O., Kinny. P., 2003. Atlas of zircon textures, in: Hanchar, J.M., Hoskin, P.W.O. (Eds.), Zircon. Rev. Mineral. Geochem., v. 53, pp. 469-500.

Da Costa, G.V., 2008. Química mineral e geotermobarometria de xenólitos mantélicos do kimberlito Canastra-01. Master thesis (Dissertação de Mestrado no. 239). Instituto de Geociências, Universidade de Brasília.

Davis, G. L., 1977. The ages and uranium contents of zircon from kimberlites and associated rocks. Extended Abstr., 2nd Int. Kimberlite Conf., Santa Fe, New Mexico.

Dawson, J.B., Hill., P.G., Kinny, P.D., 2001. Mineral chemistry of a zircon-bearing, composite, veined and metasomatised upper-mantle peridotite xenolith from kimberlite. Contrib. Mineral. Petrol. 140 (6), 720-733.

De Araujo, A.G., Perevalov, O.V., 1998. Carta de recursos minerais - Mineral Resources Map. Ministério Geol. e Minas. Inst. Geol. Angola, Luanda.

De Araujo, A.G., Perevalov, O.V., Jukov R.A., 1988. Carta geológica de Angola - Geological Map of Angola. Scale 1 : 1 000 000. Ministèrio da Indústria. Inst. Nac. Geol., Luanda.

De Carvalho, H., Tassinari, C., Alves, P.H., 2000. Geochronological review of the Precambrian in western Angola: links with Brazil. J. Afr. Earth Sci. 31 (2), 383-402.

Egorov, K.N., Roman'ko, E.F. Podvysotsky, V.T., Sablukov, S.M, Garanin, V.K., D'yakonov, D.B, 2007. New data on kimberlite magmatism in southwestern Angola. Russian Geol. Geophys. 48 (4), 323-336.

ACCEPTED MANUSCRIPT

Eley, R., Grütter, H., Louw, A., Tunguno, C., Twidale J., 2008. Exploration Geology of the Luxinga kimberlite Cluster (Angola) with evidence supporting the presence of kimberlite lava. Extended Abstr. No. 9IKC-A-00166, 9th Int. Kimberlite Conf., Frankfurt.

Fleischer, R., 1998. A rift model for the sedimentary diamond deposits of Brazil. Miner. Deposita 33 (3), 238-254.

Griffin, W.L., Pearson, N.J., Belousova, E., Jackson, S.E., van Achterbergh, E., O'Reilly, S.Y., Shee, S.R., 2000. The Hf isotope composition of cratonic mantle: LAM-MC-ICPMS analysis of zircon megacrysts in kimberlites. Geochim. Cosmochim. Acta 64 (1), 133-147.

Griffin, W.L., Powell, W.J., Pearson, N.J., O'Reilly, S.Y., 2008. GLITTER: data reduction software for Laser Ablation ICP-MS, in: Sylvester, P. (Ed.), Laser Ablation ICP-MS in the Earth Sciences: Current Practices and Outstanding Issues, Short Course Ser., vol. 40. Mineral. Assoc. Can., Québec, pp. 308-311.

Grütter, H.S., Gurney, J.J., Menzies, A.H., Winter, F., 2004. An updated classification for mantle-derived garnet, for use by diamond explorers. Lithos, 77, 841-857.

Guiraud, R., Bosworth, W. Thierry, J. Delplanque A., 2005. Phanerozoic geological evolution of Northern and Central Africa: an overview. J. Afr. Earth Sci. 43, 83–143.

Guiraud, M., Buta-Neto, A., Quesne, D., 2010. Segmentation and differential post-rift uplift at the Angola margin as recorded by the transform-rifted Benguela and oblique-to-orthogonal-rifted Kwanza basins. Mar. Pet. Geol. 27, 1040–1068.

ACCEPTED MANUSCRIPT

Haggerty, S.E., 1991. Oxide mineralogy of the Upper Mantle, in: Lindsley, D.H. (Ed.), Oxide Minerals: petrologic and magnetic significance. Rev. Mineral., vol. 25, Chantilly, pp. 355–416.

Haggerty, S.E., Raber, E. Naeser, C.W., 1983. Fission track dating of kimberlitic zircons. Earth Planet. Sci. Lett. 63 (1), 41-50.

Hamilton, M.A., Pearson, D.G., Stern, R.A., Boyd, F.R., 1998. Constraints on MARID petrogenesis: SHRIMP II U–Pb zircon evidence for pre-eruption metasomatism at Kampfersdam. Extended Abstr., 7th International Kimberlite Conference, Cape Town, pp. 296-298.

Hawkesworth, C.J., Gallagher, K., Kelley, S., Mantovani, M., Peate, D.W., Regelous, M., Rogers N.W., 1992. Parana magmatism and the opening of the South Atlantic, in: Storey, B.C., Alabaster, T., Pankhurst, R.J (Eds.), Magmatism and the causes of continental break-up. Geol. Soc. Spec. Publ. No. 68, London, pp. 221-240.

Hawkesworth, C., Kelley, S., Turner, S., Le Roex, A., Storey, B., 1999. Mantle processes during Gondwana break-up and dispersal. J. Afr. Earth Sci. 28 (1), 239-261.

Heaman, L.M., Creaser, R.A., Cookenboo, H.O., Chacko, T., 2006. Multi-stage modification of the northern Slave mantle lithosphere: Evidence from zircon- and diamond-bearing eclogite xenoliths entrained in Jericho Kimberlite, Canada. J. Petrol. 47 (4), 821-858.

Hoskin, P.W.O., Schaltegger, U., 2003. The composition of zircon and igneous and metamorphic petrogenesis, in: Hanchar, J.M., Hoskin, P.W.O. (Eds.), Zircon. Rev. Mineral. Geochem., v. 53, pp. 27-62.

ACCEPTED MANUSCRIPT

Jackson, S., 2008. Calibration strategies for elemental analysis by LA-ICP-MS, in: Sylvester, P. (Ed.), Laser Ablation ICP-MS in the Earth Sciences: Current Practices and Outstanding Issues, Short Course Ser., vol. 40. Mineral. Assoc. Can., Québec, pp. 169-188.

Jelsma, H., Barnett, W., Richards, S., Lister, G., 2009. Tectonic setting of kimberlites. Lithos 112S, 55-165.

Jelsma, H.A., de Wit, M.J., Thiart, C., Dirks, P.H.G.M., Viola, G., Basson, I.J., Anckar, E., 2004. Preferential distribution along transcontinental corridors of kimberlites and related rocks of Southern Africa. S. Afr. J. Geol. 107, 301-324.

Jelsma, H., Krishnan, U., Perrit, S., Preston, R., Winter, F., Lemotlo, L., v/d Linde, G., Armstrong, R., Phillips, D., Joy, S., Costa, J., Facatino, M., Posser, A., Kumar, M., Wallace, C., Chinn, I., Henning, A., 2012. Kimberlites from Central Angola: a case study of exploration findings. Extended Abstr. No. 10IKC-42, 10th International Kimberlite Conference, Bangalore, pp. 1-5.

Jochum, K.P., Stoll, B., 2008. Reference materials for elemental and isotopic analyses by LA-(MC)-ICP-MS: successes and outstanding needs, in: Sylvester, P. (Ed.), Laser Ablation ICP-MS in the Earth Sciences: Current Practices and Outstanding Issues, Short Course Ser., vol. 40. Mineral. Assoc. Can., Québec, pp. 147-168.

Kinny, P.D., Dawson, J.B., 1992. A mantle metasomatic injection event linked to late Cretaceous kimberlite magmatism. Nature 360, 726-728.

ACCEPTED MANUSCRIPT

Liati, A., Leander, F., Dieter, G., Fanning, C.M., 2004. The timing of mantle and crustal events in South Namibia, as defined by SHRIMP-dating of zircon domains from a garnet peridotite xenolith of the Gibeon Kimberlite Province. J. Afr. Earth Sci. 39 (3-5), 147-157.

Longerich, H.P., Jackson, S.E., Günther, D., 1996. Laser ablation inductively coupled plasma mass spectrometric transient signal data acquisition and analyte concentration calculation. J. Anal. At. Spectrom. 11, 899-904.

Mezger, K., Krogstad, E.J., 1997. Interpretation of discordant U-Pb zircon ages: An evaluation. J. Metamorph. Geol. 15, 127-140.

Moore, R.O., Griffin, W.L., Gurney, J.J., Ryan, C.G., Cousens, D.R., Sic, S.H., Suter, G.F., 1992. Trace element geochemistry of ilmenite megacrysts from the Monastery kimberlite, South Africa. Lithos 29, 1-18.

Nimis, P., Taylor, W.R., 2000. Single clinopyroxene thermobarometry for garnet peridotites. Part I. Calibration and testing of a Cr-in-Cpx barometer and an enstatite-in-Cpx thermometer. Contrib. Mineral. Petrol. 139, 514-554.

Page, F.Z., Fu, B., Kita, N.T., Fournelle, J., Spicuzza, M.J., Schulze, D.J., Viljoen, F., Basei, M.A.S., Valley, J.W., 2007. Zircons from kimberlite: New insights from oxygen isotopes, trace elements, and Ti in zircon thermometry. Geochim. Cosmochim. Acta 71 (15), 3887-3903.

Pivin, M., Féménias, O., Demaiffe, D., 2009. Metasomatic mantle origin for Mbuji-Mayi and Kundelungu garnet and clinopyroxene megacrysts (Democratic Republic of Congo). Lithos 112S, 951-960.

ACCEPTED MANUSCRIPT

Pereira, E., Rodrigues, J., Reis B., 2003. Synopsis of Lunda geology, NE Angola: implications for diamond exploration. Comun. Inst. Geol. Min. 90, 189-212.

Read, G., Grütter, H., Winter, S., Luckman, N., Gaunt, F., Thomsen, F., 2004. Stratigraphic relations, kimberlite emplacement and lithospheric thermal evolution, Quiricó Basin, Minas Gerais State, Brazil. Lithos 77, 803-818.

Reis, B., 1972. Preliminary note on the distribution and tectonic control of kimberlites in Angola. Abstr., 24th Int. Geol. Congr., Rep. Sess. 4, 276-281, Montreal.

Robles-Cruz, S.E., Watangua, M., Isidoro, L. Melgarejo, J.C., Galí, S. Olimpio, A., 2009. Contrasting compositions and textures of ilmenite in the Catoca kimberlite, Angola, and implications in exploration for diamond. Lithos 112S, 966-975.

Rudnick, R.L., Ireland, T.R., Gehrels, G., Irving, A.J., Chesley, J.T., Hanchar, J.M., 1998. Dating mantle metasomatism: U–Pb geochronology of zircons in cratonic mantle xenoliths from Montana and Tanzania. Extended Abstr., 7th International Kimberlite Conference, Cape Town, pp. 754-756.

Schärer, U., Corfu, F., Demaiffe, D., 1997. U-Pb and Lu-Hf isotopes in baddeleyite and zircon megacrysts from the Mbuji-Mayi kimberlite: constraints on the subcontinental mantle. Chem. Geol. 143, 1-16.

Stern, R.A., Amelin Y., 2003. Assessment of errors in SIMS zircon U-Pb geochronology using a natural zircon standard and NIST SRM 610 glass. Chem. Geol. 197, 111-146.

Watson, E.B., Wark, D.A., Thomas, J.B., 2006. Crystallization thermometers for zircon and rutile. Contrib. Mineral. Petrol. 151, 413-433.

ACCEPTED MANUSCRIPT

White, S.H., de Boorder, H., Smith, C.B., 1995. Structural controls of kimberlite and lamproite emplacement. J. Geochem. Explor. 53 (1-3), 245-264.

Whitehouse, M.J., Platt, J.P., 2003. Dating high-grade metamorphism-constraints from rare-earth elements in zircon and garnet. Contrib. Mineral. Petrol. 145, 61-74.

Williams, I.S., 1998. U-Th-Pb geochronology by ion microprobe, in: McKibben, M.A., Shanks III, W.C., Ridley, W.I. (Eds.), Applications of microanalytical techniques to understanding mineralizing processes, Reviews in Econ. Geol. 7, 1–35.

Wilson, M., 1992. Magmatism and continental rifting during the opening of the South Atlantic ocean: a consequence of Lower Cretaceous super-plume activity?, in: Storey, B.C., Alabaster, T., Pankhurst, R.J (Eds.), Magmatism and the causes of continental break-up. Geol. Soc. Spec. Publ. No. 68., London, pp. 241-255.

Zartman, R.E., Richardson, S.H., 2005. Evidence from kimberlitic zircon for a decreasing mantle Th/U since the Archean. Chem. Geol. 220, 263-283.

Web references

http://georem.mpch-mainz.gwdg.de/, data downloaded February 24, 2010. GeoReM is a Max Planck Institute database for reference materials of geological and environmental interest, such as rock powders, synthetic, and natural glasses as well as mineral, isotopic, biological, river water, and seawater reference materials. It contains published analytical data and compilation values (major and trace element concentrations, radiogenic and stable isotope ratios). It also contains all important metadata about the analytical values such as uncertainty,

ACCEPTED MANUSCRIPT

analytical method and laboratory. Sample information and references are also included, as well as more than 2,400 reference materials, 25,400 analyses from more than 5,000 papers, and preferred analytical values (State: 07/01/2011). It complements the three earthchem databases GEOROC, NAVDAT, PETDB.

Figure captions

Fig. 1. Location map of the area of study. Geological map of northeastern Angola (after De Araujo et al., 1988; De Araujo and Perevalov, 1998; De Carvalho et al., 2000; Egorov et al., 2007). Abbreviations: Quaternary (QQ), Cenomanian (CE), Albian (AB), Permian (PP), Carboniferous (CC), Undifferentiated (Undiff.), Group (Gp), Formation (Fm), sandstone (Sst), conglomerate (Cgl), limestone (Lst), marlstone (Mrls), argillaceous limestone (ArgLst), claystone (Clst), granite (Gr), gabbro (Gb), quartzite (Qzt), schist (Sch), granodiorite (Grdr), dolerite (Do), amphibolite (Am), gneiss (Gns), carbonatites (Cbt), nephelite (Nph), syenite (Syt), ijolite (Ijt), pyroxenite (Pxt), anorthosite (Ant), troctolite (Trt), Norite (Nrt), epidotite (Epd), granulite (Gnt), eclogite (Ecl).

Fig. 2. Representative crystals of zircon from the Catoca kimberlite and one crystal from the Tchiuzo pipe. (A) Back-scattered electron image of zircon (Zrn) and baddeleyite (Bdl) crystals from the Catoca kimberlite, crystal no. 10. (B) Cathodoluminescence image of crystal no. 10 at a different scale than A. (C, D, and E) Cathodoluminescence images of crystals of zircon (nos. 12, 4, and 18, respectively) from the Catoca pipe, and (F) crystal of zircon (no. 20) from the Tchiuzo pipe.

ACCEPTED MANUSCRIPT

Fig. 3. Chondrite-normalized REE patterns (in black) for the three crystals of zircon (nos. 19, 21, and 22) from the Catoca kimberlite. Open symbols represent the rim, and closed symbols represent the core of crystals. Gray lines represent average REE trends for zircon from kimberlites and carbonatites reported by others and included here for comparative purposes.

Fig. 4. Weighted mean of $^{206}Pb/^{238}U$ ages of zircon. (A) Zircon from the Catoca and the Tchiuzo kimberlites. (B) Zircon from the Catoca kimberlite.

Fig. 5. Tera-Wasserburg (T-W) diagrams with data obtained from zircon crystals from the Catoca and Tchiuzo kimberlites. Ellipses in gray are those that have a high proportion of ^{204}Pb.

(A) T-W diagram with data of crystals from the Catoca kimberlite, intersecting at 117.70 ± 0.94 Ma. (B) T-W diagram with data of crystals from the Tchiuzo kimberlite, intersecting at 120.4 ± 2.8 Ma.

Fig. 6. Th versus U concentration in zircon from the Catoca (black circles) and the Tchiuzo pipes (gray circles). The area in light gray corresponds to the field of mantle-derived zircon megacrysts, as defined by Heaman et al. (2006). The dashed square represents the characteristic concentration of zircon in kimberlitic rocks reported by Belousova et al. (2002). A black star on the border of some circles indicate that those analyses were performed on zircon crystals with a rim of baddeleyite. Crystals of zircon outside the mantle-derived field are enriched in U and Th.

ACCEPTED MANUSCRIPT

Most of the crystals are larger than 0.6 mm in size, fractured, and yield similar ages. There is no correlation between age and Th/U content.

Fig. 7. Summary of geochronological results (SHRIMP) for the Catoca kimberlite eruption.

Tables

Table 1. Description of zircon crystals analyzed by SHRIMP.

Table 2. LA-ICP-MS operating conditions and data-acquisition parameters.

Table 3. Results of Laser-ablation ICP-MS analyses of zircon from the Catoca kimberlite.

Table 4. Summary of SHRIMP data for zircon from the Catoca and Tchiuzo kimberlites.

ACCEPTED MANUSCRIPT

ACCEPTED MANUSCRIPT

Table 1. Description of zircon crystals analyzed by SHRIMP.

Kimberlite	Borehole	Sample name/ Mount	Type of sample	Crystal No.	Width (µm)	Length (µm)	Crystal border	Zonation (using cathodoluminescence images)	Presence of rim of baddeleyite	Degree of fracturing	Type of analyses
Catoca	535	CA-535-379-29B	core (TK)	1	350	600	angular	oscillatory	YES	L	SHRIMP
				2	120	1000	subangular	patchy zoning	YES	M	SHRIMP
Catoca	335	CA-335-601	concentrate	3	900	1100	subrounded	patchy?-oscillatory zone core	NO	M	SHRIMP
				4	800	1000	subrounded	oscillatory	NO	L	SHRIMP
				5	550	650	angular	oscillatory	NO	VL	SHRIMP
				6	650	1100	subrounded	oscillatory-patchy rim	NO	VL	SHRIMP
				7	800	800	subangular	oscillatory	NO	VL	SHRIMP
				8	600	800	subangular	oscillatory	NO	M	SHRIMP
				9	800	850	subangular	no zoning	YES	M	SHRIMP
Catoca	535	CA-535-359-27BA	core (TK)	10	450	850	angular	oscillatory	YES	L	SHRIMP
Catoca	335	CA-335-551	concentrate	11	600	1000	subrounded	oscillatory	NO	L	SHRIMP
				12	800	850	subangular	oscillatory	NO	VL	SHRIMP
				13	750	1450	subrounded	oscillatory-patchy by sectors	NO	L	SHRIMP
				14	700	800	subangular	oscillatory and patchy in fracture	NO	M	SHRIMP
				15	400	1150	subrounded	oscillatory	NO	M	SHRIMP
				16	500	650	subangular	oscillatory	NO	VL	SHRIMP
				17	400	680	angular	oscillatory	NO	VL	SHRIMP
Catoca	535	CA-535-350-26	core (TK)	18	3800	4000	subrounded	growth zoning with a patchy	NO	M	SHRIMP
Catoca	536	CA-536-304	concentrate	19	1400	2200	subangular	oscillatory	NO	M	SHRIMP + LA-ICP-MS
				21	1500	1300	subrounded	NA	NO	L	LA-ICP-MS
				22	1200	1000	subrounded	NA	NO	L	LA-ICP-MS
Tchiuzo	G10	TZ-G10-13	concentrate	20	550	980	subangular	oscillatory	NO	M	SHRIMP

Middle (M)= 40-20% of fractures; Low (L)= 5-20%; Very Low (VL)= less than 5%.

ACCEPTED MANUSCRIPT

Table 2. LA-ICP-MS operating conditions and data-acquisition parameters.

LA	
Model	New Wave Research UP213
Wavelength	213 nm
Pulse duration (FWHM)	ca. 4 ns
Nominal spot sizes used	80-120 µm
Repetition rate	10 Hz
Energy density at sample	*ca.* 5 J/cm^2
ICP-MS	
Model	Perkin Elmer ELAN 6100DRC
Carrier has flow (He)	0.96 L/min
Make-up flow (Ar)	0.70 L/min
Sampler and skimmer	Nickel
Data-acquisition parameters	
Data-acquisition protocol	Time-Resolved Analysis
Detector mode	Pulse counting (< 3 M c.p.s.)
Isotopes determined	^{25}Mg, ^{29}Si, ^{39}K, ^{42}Ca, ^{49}Ti, ^{51}V, ^{53}Cr, ^{55}Mn, ^{57}Fe, ^{59}Co, ^{60}Ni, ^{65}Cu, ^{66}Zn, ^{71}Ga, ^{72}Ge, ^{85}Rb, ^{88}Sr, ^{89}Y, ^{90}Zr, ^{93}Nb, ^{133}Cs, ^{137}Ba, ^{139}La, ^{140}Ce, ^{141}Pr, ^{146}Nd, ^{147}Sm, ^{151}Eu, ^{157}Gd, ^{159}Tb, ^{163}Dy, ^{165}Ho, ^{167}Er, ^{169}Tm, ^{173}Yb, ^{175}Lu, ^{177}Hf, ^{181}Ta, ^{205}Tl, ^{206}Pb, ^{207}Pb, ^{208}Pb, ^{232}Th, ^{238}U
Scanning mode	Peak hopping, 1 point per peak
Dwell time per isotope	10 ms
Time per mass sweep	*ca.* 453 ms
Data acquisition time	180 s (*ca.* 60 s gas blank, up to *ca.* 120 s ablation)
Oxide production	ThO^+/Th^+ <1%
Standards and calibration	
Samples	Polished 25 mm round mounts
Data-processing software	GLITTER 4.4.2 (Griffin et al., 2008)
Calibration standard	NIST SRM 610, GEOREM Preferred Values, Feb. 2010
Internal standard	SiO2 (32.8 wt%)
Secondary standard	USGS microbeam standard, BCR-2G

ACCEPTED MANUSCRIPT

Table 3. Results of Laser-ablation ICP-MS analyses of zircon from the Catoca kimberlite.

Kimberlite	Catoca	Catoca	Catoca	Catoca	Catoca
Crystal No.	22	22	21	21	19
Type of sample	Concentrate	Concentrate	Concentrate	Concentrate	Concentrate
Spot location	core	core	core	rim	core
Sample number	fe26b05	fe26b06	fe26b09	fe26b10	fe26b15
All values are reported in ppm					
Ti	5.4	10.9	1.17	2.66	3.4
Sr	0.045	2.85	0.34	0.61	0.61
Y	46	120	330	480	39
Nb	1.25	4.1	8.8	13.5	0.86
Ba	0.088	4.3	0.59	1.34	0.38
La	0.0181	0.50	0.054	0.168	0.075
Ce	0.79	2.89	5.3	9.6	0.82
Pr	0.031	0.211	0.187	0.39	0.0264
Nd	0.39	1.12	2.64	5.5	0.214
Sm	0.73	1.04	4.4	7.7	0.241
Eu	0.44	0.64	2.89	5.0	0.243
Gd	2.66	4.4	17.3	28.5	1.03
Tb	0.76	1.50	5.2	8.0	0.52
Dy	6.5	16.2	51	79	5.1
Ho	1.96	5.0	15.2	22.8	1.69
Er	6.4	17.7	54	77	6.2
Tm	1.13	3.2	10.4	14.9	1.41
Yb	8.8	25.4	86	123	12.9
Lu	1.42	3.8	11.7	15.1	1.50
Hf	12,800	13,700	9,180	9,970	9,580
Th	2.90	9.3	47	78	2.04
U	7.9	26.8	112	152	10.0

ACCEPTED MANUSCRIPT

Table 4. Summary of SHRIMP data for zircon from the Catoca and Tchiuzo kimberlites.

Kimberlite	Crystal No.	Spot name	U (ppm)	Th (ppm)	Th/U	$^{206}Pb^*$ (ppm)	$f(206)^{204}$ %	Total $\frac{^{238}U}{^{206}Pb}$	204Pb Corrected Ratios $\frac{^{207}Pb}{^{206}Pb}$	204Pb Corrected Ratios $\frac{^{207}Pb}{^{235}U}$	$\frac{^{206}Pb}{^{238}U}$	207 corrected Age (Ma) $\frac{^{206}Pb}{^{238}U}$
Catoca	2	10001-2.1	82	43	0.52	1.3	0.73	53.756 ± 0.705	0.0537 ± 0.0017	0.1210 ± 0.0068	0.0185 ± 0.0002	118.1 ± 1.6
		10001-2.2	72	34	0.47	1.1	2.12	54.013 ± 0.719	0.0491 ± 0.0017	0.0769 ± 0.0234	0.0181 ± 0.0003	118.2 ± 1.6
		10001-2.3	23	6	0.28	0.3	2.45	54.672 ± 0.901	0.0596 ± 0.0036	0.0950 ± 0.0480	0.0178 ± 0.0005	115.3 ± 2.0
Catoca	3	10002-2a.1	166	137	0.82	2.7	1.69	52.986 ± 0.603	0.0536 ± 0.0012	0.1001 ± 0.0185	0.0186 ± 0.0003	119.8 ± 1.4
		10002-2a.2	132	136	1.03	2.1	1.24	53.490 ± 0.660	0.0550 ± 0.0014	0.1132 ± 0.0241	0.0185 ± 0.0003	118.5 ± 1.5
		10002-2a-3.1	112	108	0.97	1.8	0.58	53.148 ± 0.597	0.0579 ± 0.0016	0.1368 ± 0.0060	0.0187 ± 0.0002	118.8 ± 1.3
Catoca	4	10002-2b.3	14	3	0.21	0.2	5.14	49.764 ± 0.896	0.1095 ± 0.0061	0.1760 ± 0.2517	0.0191 ± 0.0022	119.1 ± 2.3
		10002-2b.4	22	5	0.23	0.3	9.51	51.720 ± 0.659	0.0957 ± 0.0046	0.0283 ± 0.1018	0.0175 ± 0.0009	116.6 ± 1.6
Catoca	5	10002-3a.3	14	5	0.34	0.2	3.33	49.902 ± 1.304	0.1212 ± 0.0065	0.2526 ± 0.1009	0.0194 ± 0.001	117.0 ± 3.2
		10002-3a.4	28	11	0.38	0.4	8.94	54.638 ± 0.783	0.0585 ± 0.0032	0.0543 ± 0.0711	0.0167 ± 0.0013	115.5 ± 1.7
Catoca	6	10002-3b.4	28	7	0.27	0.4	13.06	52.131 ± 0.644	0.0739 ± 0.0036	0.1137 ± 0.0240	0.0167 ± 0.0008	118.8 ± 1.6
Catoca	8	10002-4b.1	9	2	0.23	0.2	-8.35	51.392 ± 1.433	0.0561 ± 0.0067	0.3509 ± 0.0996	0.0211 ± 0.0011	123.1 ± 3.5
Catoca	9	10002-4c.1	147	122	0.83	2.3	0.38	54.191 ± 0.712	0.0517 ± 0.0013	0.1227 ± 0.0182	0.0184 ± 0.0003	117.4 ± 1.5
		10002-4c.2	177	184	1.04	2.8	0.91	54.663 ± 0.613	0.0483 ± 0.0011	0.1014 ± 0.0158	0.0181 ± 0.0002	116.9 ± 1.3
Catoca	10	10003-1.3	45	18	0.41	0.7	3.72	52.795 ± 0.702	0.0557 ± 0.0024	0.0587 ± 0.0623	0.0182 ± 0.0006	119.9 ± 1.6
		10003-1.4	34	15	0.44	0.5	4.78	54.605 ± 0.695	0.0483 ± 0.0027	0.0141 ± 0.0799	0.0174 ± 0.0007	117.0 ± 1.5
Catoca	11	10004-1a.1	11	2	0.21	0.2	11.21	48.272 ± 0.706	0.1342 ± 0.0083	0.0967 ± 0.3592	0.0184 ± 0.003	118.9 ± 2.2
Catoca	12	10004-1b.1	48	18	0.38	0.7	6.65	53.216 ± 0.638	0.0722 ± 0.0027	0.0327 ± 0.0413	0.0175 ± 0.0004	116.7 ± 1.4
		10004-1b.2	51	18	0.34	0.8	6.16	54.479 ± 0.638	0.0695 ± 0.0025	0.0363 ± 0.0357	0.0172 ± 0.0004	114.3 ± 1.4
Catoca	13	10004-1c.1	8	3	0.34	0.1	5.80	52.747 ± 1.850	0.0740 ± 0.0088	0.0578 ± 0.1341	0.0179 ± 0.0013	117.4 ± 4.3
Catoca	14	10004-3a.2	35	12	0.36	0.5	6.09	50.972 ± 0.752	0.0860 ± 0.0035	0.0851 ± 0.0711	0.0184 ± 0.0007	119.7 ± 1.8
Catoca	15	10004-3d.1	50	16	0.32	0.8	2.60	53.818 ± 0.631	0.0697 ± 0.0026	0.1190 ± 0.0473	0.0181 ± 0.0005	115.7 ± 1.4
		10004-3d.2	50	15	0.31	0.8	4.69	54.477 ± 0.965	0.0613 ± 0.0032	0.0490 ± 0.0596	0.0175 ± 0.0006	115.5 ± 2.1
Catoca	16	10004-4a.1	22	7	0.33	0.3	11.77	51.562 ± 0.836	0.0978 ± 0.0046	0.0202 ± 0.0805	0.0171 ± 0.0008	116.7 ± 2.0
		10004-4a.2	12	3	0.29	0.2	9.11	47.685 ± 1.070	0.1484 ± 0.0082	0.1934 ± 0.2182	0.0191 ± 0.0020	118.1 ± 2.9
Catoca	17	10004-4c.1	187	118	0.63	3.0	1.19	52.565 ± 0.582	0.0532 ± 0.0012	0.1118 ± 0.0203	0.0188 ± 0.0003	120.8 ± 1.3
		10004-4c.2	154	88	0.57	2.5	1.70	51.665 ± 0.603	0.0572 ± 0.0013	0.1121 ± 0.0162	0.0190 ± 0.0003	122.3 ± 1.4
Catoca	18	10006-1.1	197	320	1.62	3.2	0.95	53.159 ± 0.608	0.0516 ± 0.0011	0.1117 ± 0.0122	0.0186 ± 0.0002	119.7 ± 1.4
		10006-1.2	301	623	2.07	4.7	0.40	54.320 ± 0.656	0.0538 ± 0.0009	0.1276 ± 0.0073	0.0183 ± 0.0002	116.8 ± 1.4
		10006-1.3	184	315	1.71	2.9	0.67	53.863 ± 0.649	0.0577 ± 0.0012	0.1323 ± 0.0074	0.0184 ± 0.0002	117.3 ± 1.4
		10006-1.4	326	654	2.01	5.2	0.87	53.724 ± 0.589	0.0508 ± 0.0008	0.1106 ± 0.0075	0.0185 ± 0.0002	118.5 ± 1.3
Catoca	19^	10007-4.1	22	5	0.24	0.3	8.14	54.344 ± 0.694	0.0568 ± 0.0037	0.0407 ± 0.0436	0.0169 ± 0.0007	116.4 ± 1.6
		10007-4.2	79	50	0.64	1.2	3.08	54.340 ± 0.627	0.0502 ± 0.0017	0.0574 ± 0.0553	0.0178 ± 0.0005	117.3 ± 1.4
		10007-4.3	36	11	0.30	0.6	2.87	54.263 ± 0.758	0.0579 ± 0.0028	0.0820 ± 0.0514	0.0179 ± 0.0005	116.4 ± 1.7
Tchiuzo	20	10005-1.1	61	34	0.56	0.9	3.30	53.402 ± 0.731	0.0486 ± 0.0020	0.0492 ± 0.0443	0.0181 ± 0.0004	119.6 ± 1.7
		10005-1.3	36	11	0.30	0.6	9.14	49.382 ± 0.621	0.0937 ± 0.0035	0.0331 ± 0.0732	0.0184 ± 0.0006	122.4 ± 1.6
		10005-1.4	43	13	0.31	0.7	5.56	49.454 ± 0.587	0.0974 ± 0.0034	0.1329 ± 0.1156	0.0191 ± 0.0010	121.7 ± 1.5

Spot name follows the convention x-y.z; where x = sample number, y = grain number and z = spot number. Multiple analyses in an individual spot are labelled as x-y.z.z

Uncertainties reported at 1σ and are calculated by using SQUID 2.22.08.04.30, rev. 30 Apr 2008

$f206^{204}$ refers to mole percent of total 206Pb that is due to common Pb, calculated using the 204Pb-method; common Pb composition used is the surface blank (4/6: 0.05770; 7/6: 0.89500; 8/6: 2.13840)

* refers to radiogenic Pb (corrected for common Pb using measured 204Pb)

Calibration standard 6266; U = 910 ppm; Age = 559 Ma; 206Pb/238U = 0.09059

Error in $^{206}Pb/^{238}U$ calibration 1.1% (included)

Standard Error in Standard calibration was 0.30% (not included in above errors but required when comparing data from different mounts).

^ = also analyzed with LA-ICP-MS

ACCEP

ACCEPTED MANUSCRIPT

Highlights

>The SHRIMP results define a single weighted mean age of 117.9 ± 0.7 Ma.
>This U-Pb age is interpreted as the maximum age of the kimberlite eruption at Catoca.
>This event is restricted to the time between the middle of the Aptian and the Albian.
>The U/Th values suggest at least two different sources (depleted, enriched) of zircon.
>The new interpretation will be an important guide in future exploration for diamonds.

ACCEPTED MANUSCRIPT

ACCEPTED MANUSCRIPT

Figure 1

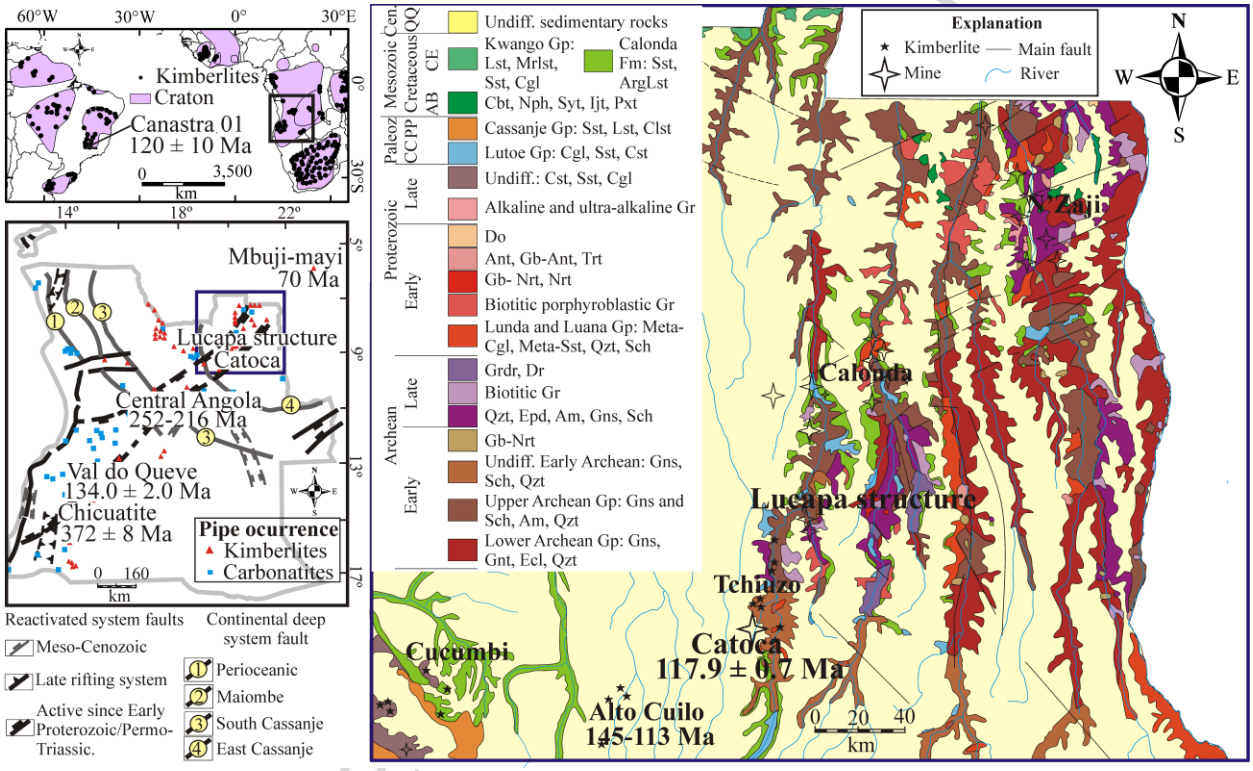

ACCEPTED MANUSCRIPT

Figure 2

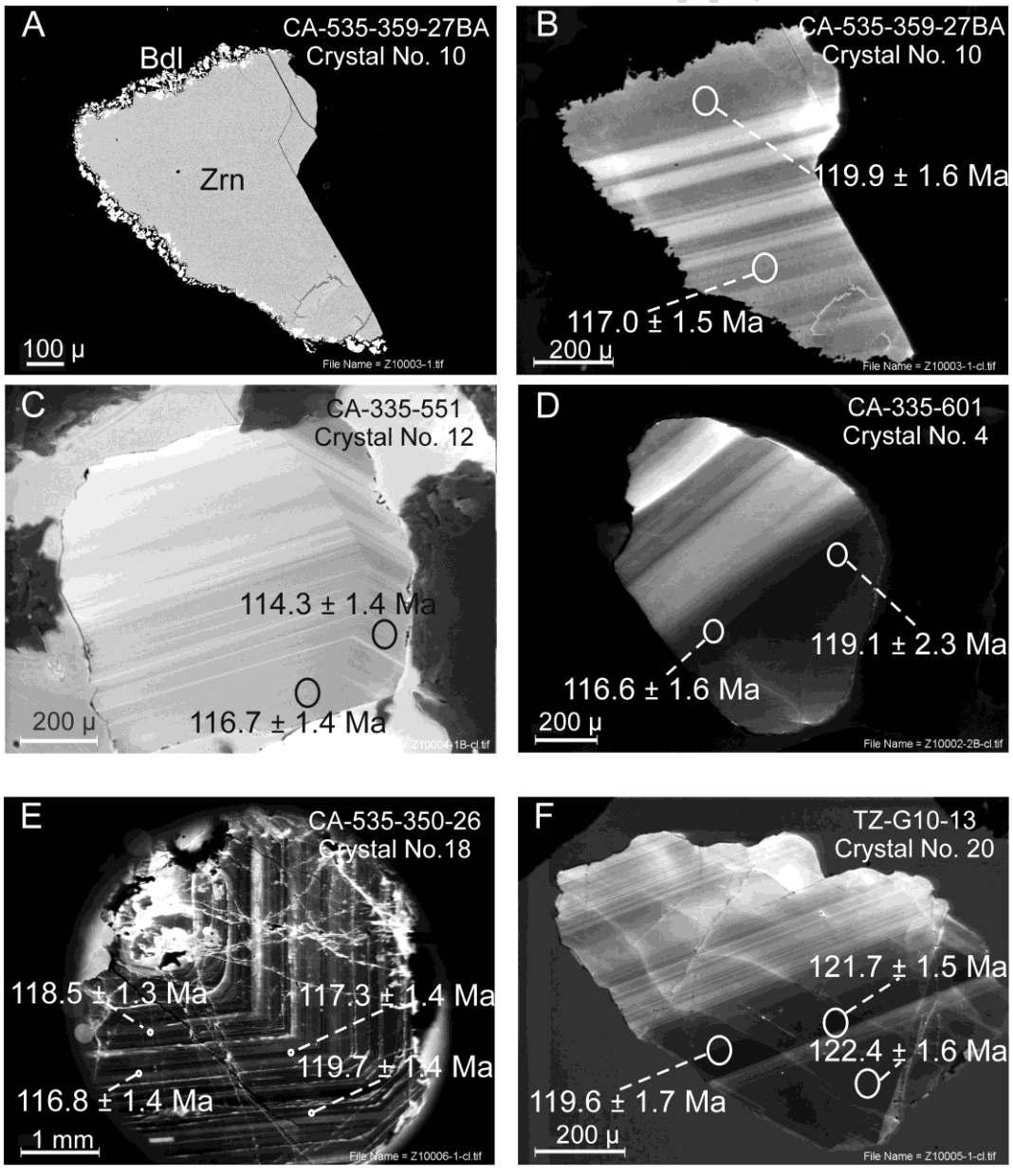

ACCEPTED MANUSCRIPT

Figure 3

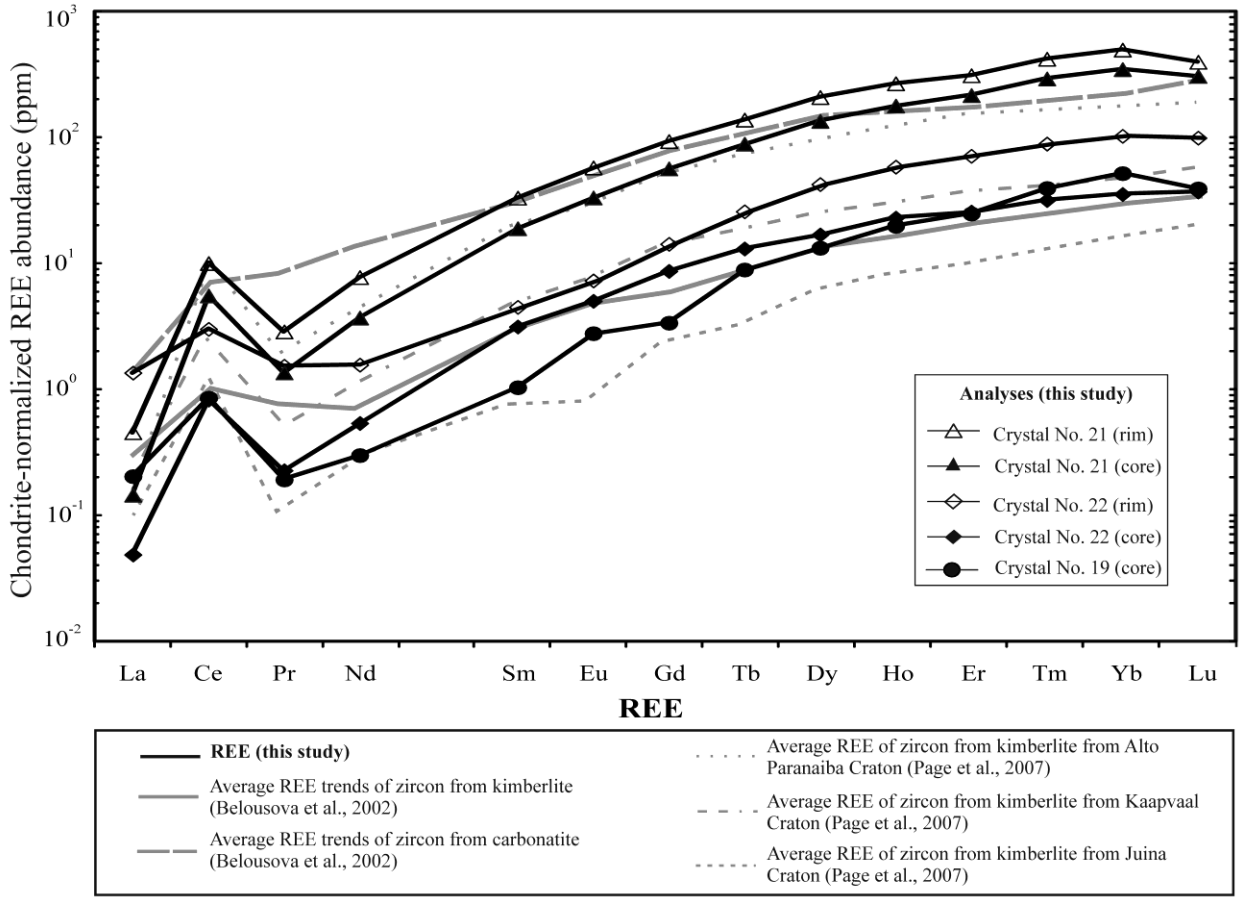

ACCEPTED MANUSCRIPT

Figure 4

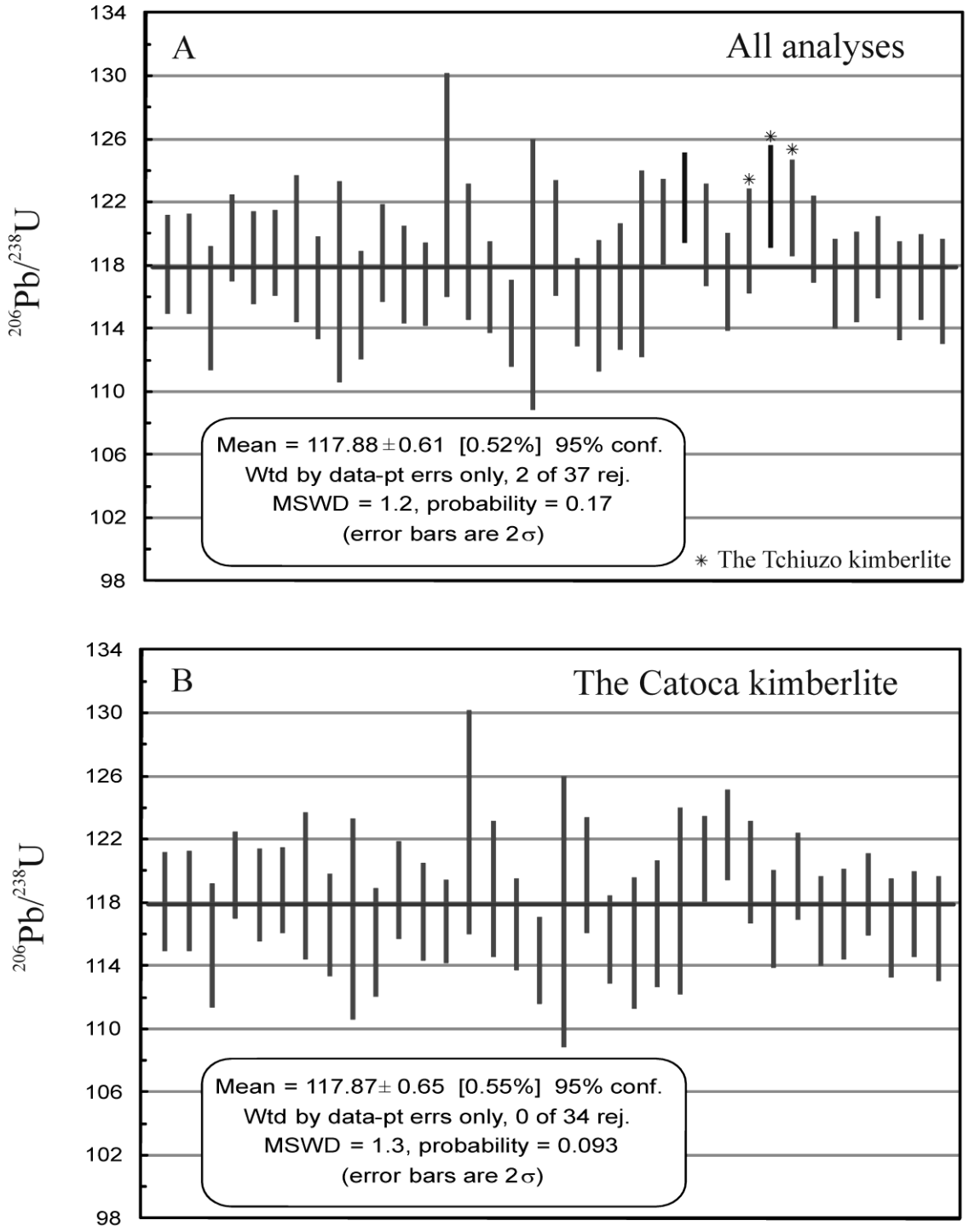

ACCEPTED MANUSCRIPT

Figure 5

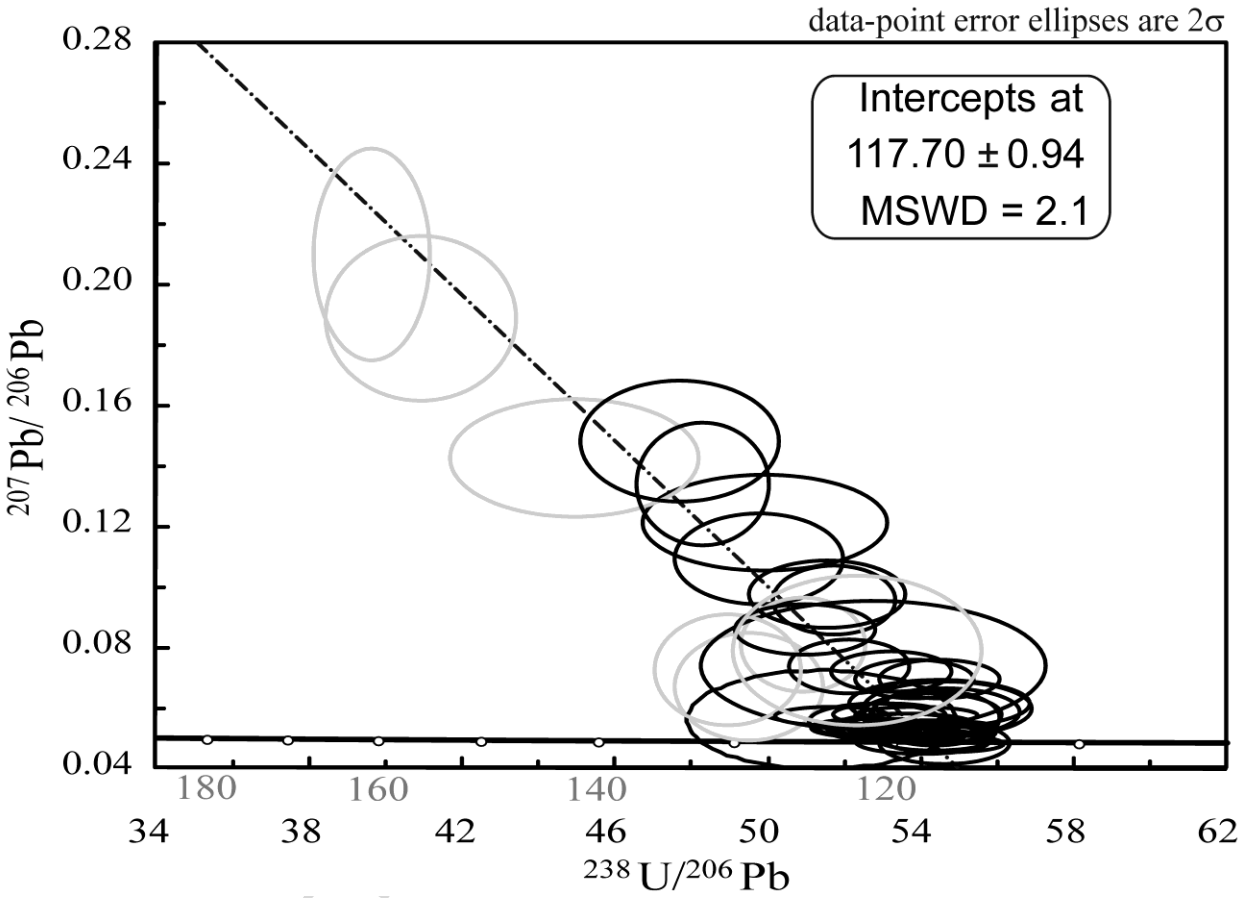

ACCEPTED MANUSCRIPT

Figure 6

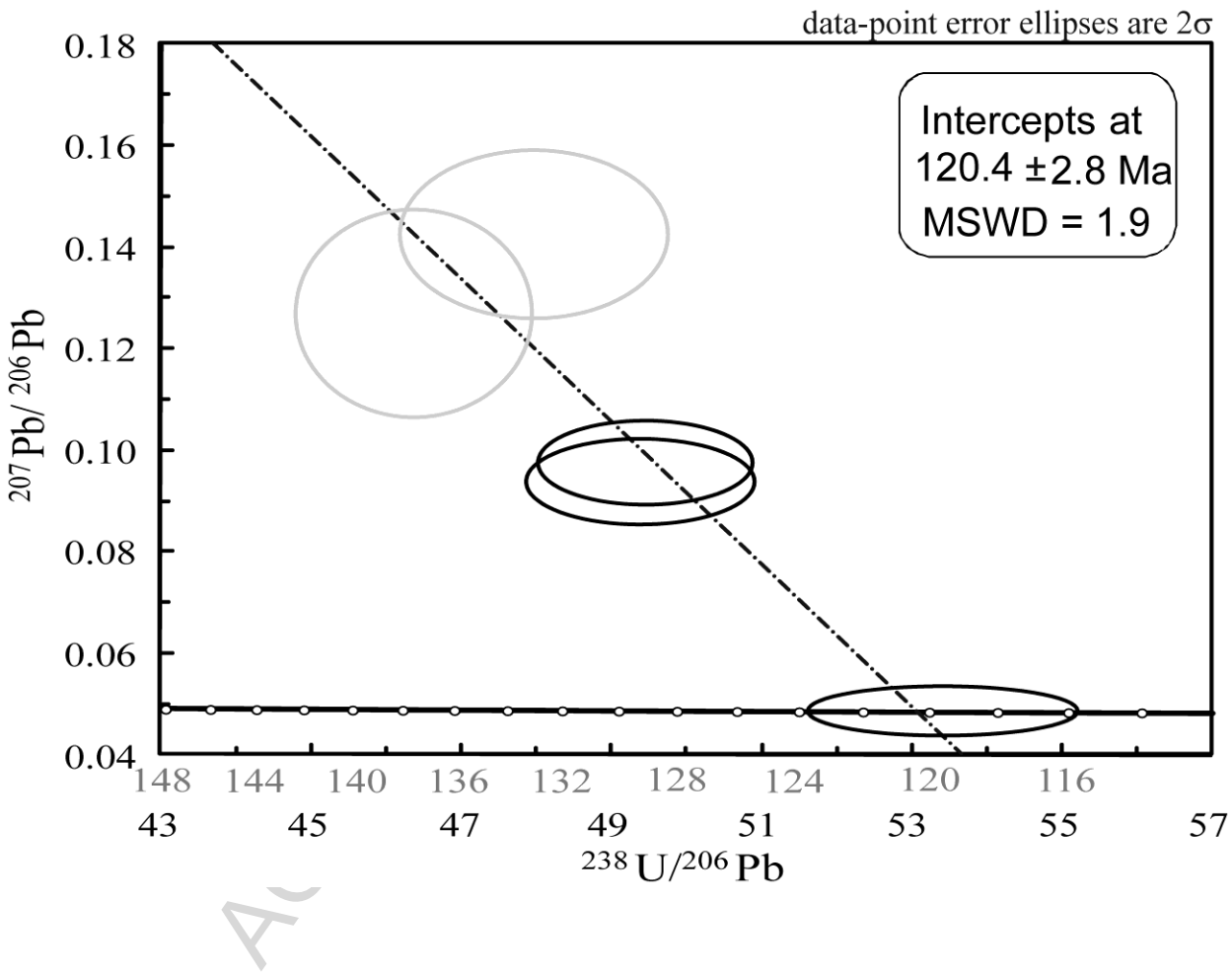

ACCEPTED MANUSCRIPT

Figure 7

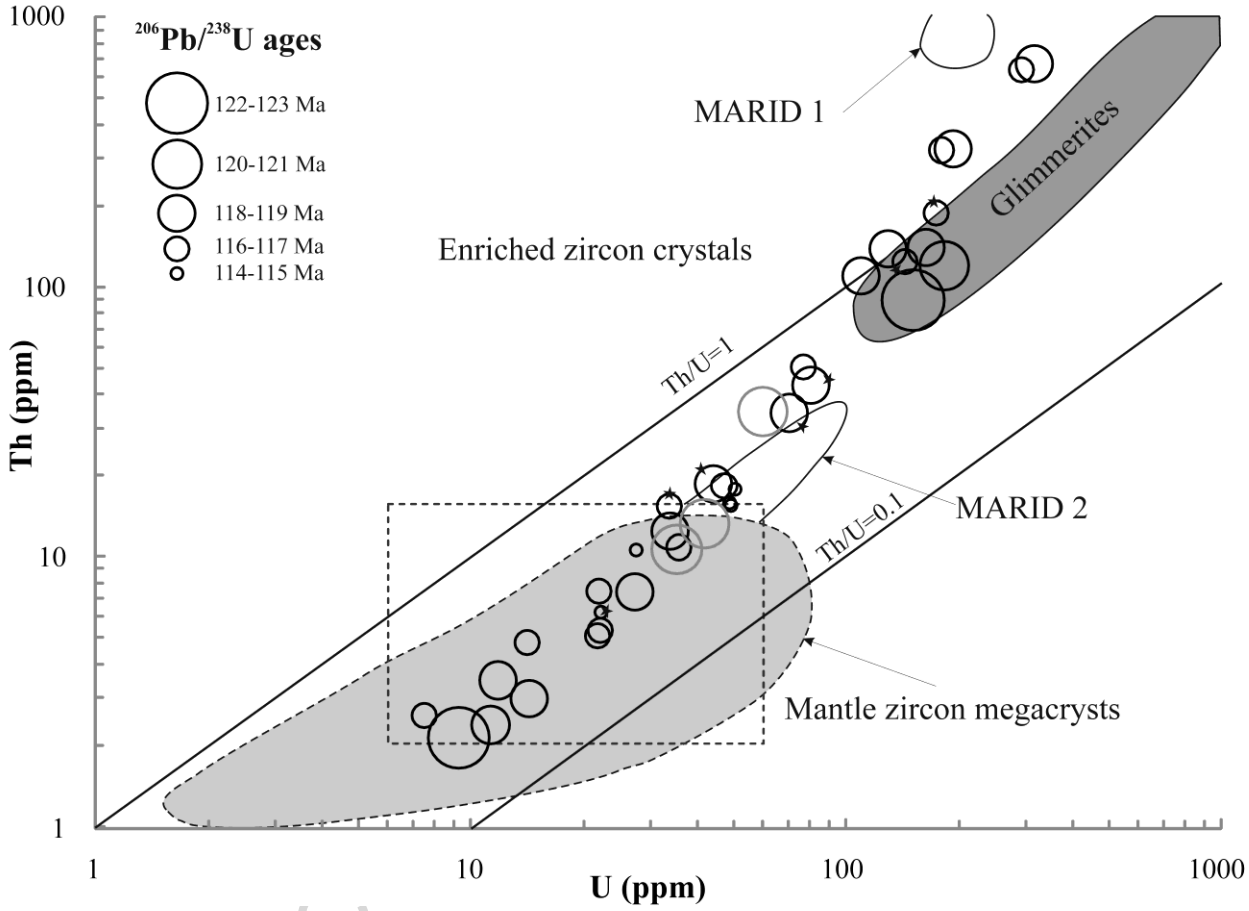

ACC

ACCEPTED MANUSCRIPT
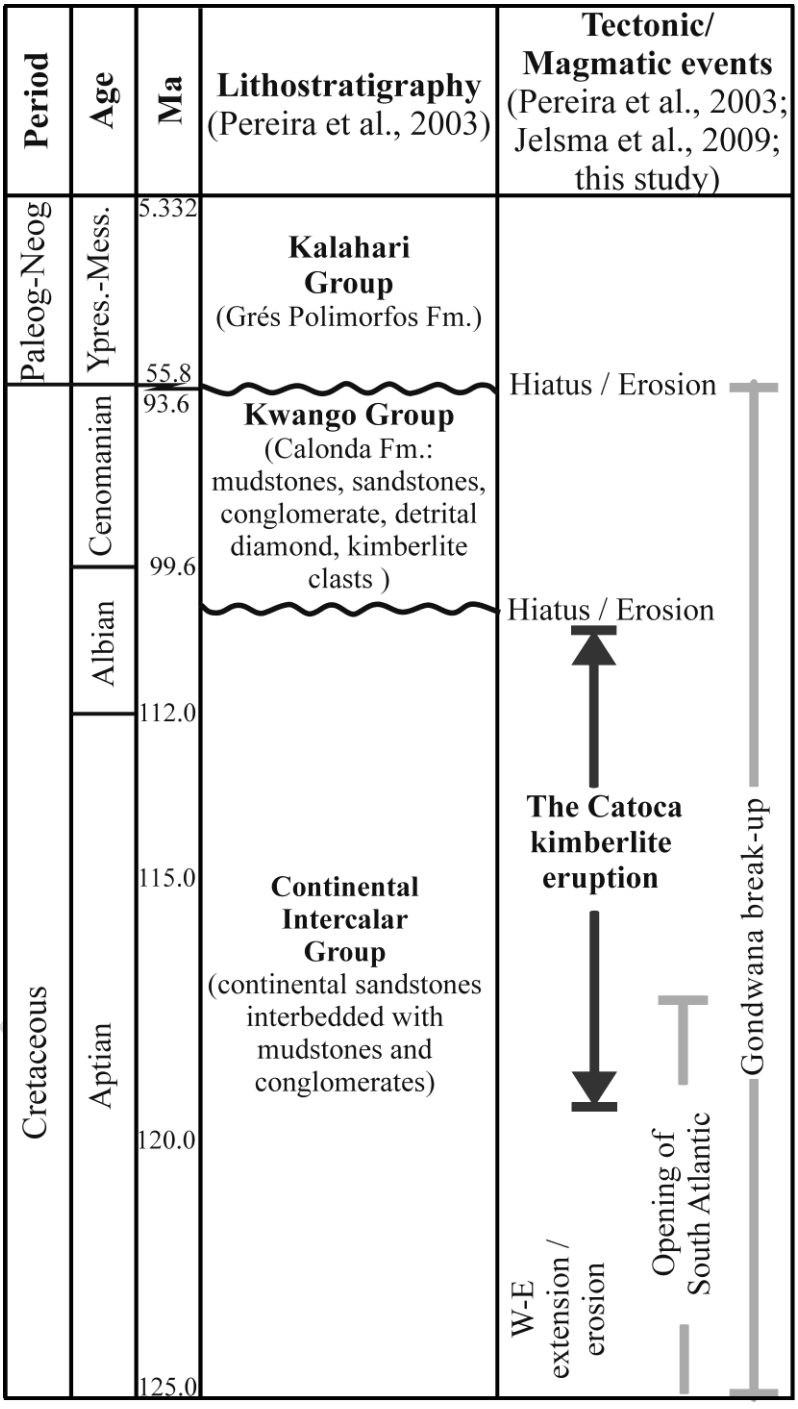
Figure 8